Final Technical Report

USGS Award 00HQGR0020

CONSTRAINTS ON CRUSTAL AND FAULT-ZONE RHEOLOGY FROM EARTHQUAKE MECHANISMS

P.I. Gregory C. Beroza
Co-P.I. Goetz H. R. Bokelmann

Program Element II. Earthquake Physics and Effects

Research supported by the U.S. Geological Survey (USGS), Department of the Interior, under USGS award number 02-HQ-GR-0020. The views and conclusions contained in this document are those of the authors and should not be interpreted as necessarily representing the official policies, either expressed or implied, of the U.S. Government.

Award # 00-HQ-GR-0020

CONSTRAINTS ON CRUSTAL AND FAULT-ZONE RHEOLOGY FROM EARTHQUAKE MECHANISMS

Gregory C. Beroza
Department of Geophysics
397 Panama Mall
Stanford, CA, 94305-2215

Phone: (650) 723-4958
Fax: (650) 725-7344
beroza@geo.stanford.edu

Technical Abstract

The traction free boundary condition across the Earth's surface provides an opportunity for studying the relationship between stress orientation and earthquake focal mechanisms because it requires alignment of principal stress axes with vertical and horizontal orientations. Our survey of earthquake focal mechanisms in Northern California found that their principal axes are also closely aligned with the vertical and the horizontal in the upper few km of the Earth's crust. Thus, the signature of the free surface boundary condition on stress also appears in focal mechanism orientations. We characterize the focal mechanism alignment by the relative magnitude of the off-diagonal elements of the seismic moment tensor. Values near the Earth's surface are small, but increase with depth to a maximum between 5 and 8 km. At greater depths there is a gradual decrease, which suggests decreasing horizontal shear traction towards the base of the seismogenic zone. We interpret this tendency of axes to become oriented near the base of the seismogenic zone as the signature of a weak zone in the lower crust. In the research sponsored under this grant, we have used this information to try to constrain the strength of the San Andreas Fault as a function of depth in the Earth's crust.

We attempt to constrain the strength of major earthquake faults in Northern California through studying the orientation at which failure occurs in microearthquakes as determined by earthquake focal mechanisms. That angle relative to the stress field can in principle constrain the coefficient of friction. We study dip angles of the rupturing fault patches and assume that those dip angles are optimally oriented with respect to the stress field. Under that assumption we obtain small values of friction at essentially all depths in the upper crust where seismicity occurs. This suggests that the major faults are weak, as has been suggested previously based on the lack of a heat-flow anomaly and nearly-perpendicular direction of the maximum principal stress.The upper bound of friction coefficient that we obtain is quite similar to the upper bound of *Lachenbruch and Sass* [1992] within which both heat-flow data and stress constraints can be reconciled.

Award # 00-HQ-GR-0020
Constraints on Crustal and Fault-Zone Rheology from Earthquake Mechanisms

Gregory C. Beroza
Department of Geophysics
397 Panama Mall
Stanford, CA, 94305-2215

Phone: (650) 723-4958
Fax: (650) 725-7344
beroza@geo.stanford.edu

Non-Technical Abstract

Laboratory measurements of rock friction suggest that earthquake faulting should generate a great deal of heat and that this ought to lead to a temperature anomaly near major faults; however, no such anomaly has been observed. We have shown that the sense of slip in small earthquakes reflects the stress field for shallow earthquakes that occur near the Earth's surface. We have used this information to try to constrain the strength of the San Andreas Fault as a function of depth in the Earth's crust. By measuring the slip angle relative to the stress field we can, in principle, constrain the coefficient of friction. We find small values of friction at essentially all depths in the upper crust where seismicity occurs, which confirms that the major faults are weak. The values we obtain are consistent with results from a previous study that were based primarily on theoretical considerations.

Introduction

A central goal of seismology is to understand the nature of faulting. One key question in this context is how strong faults are, that is, how much they resist the motion of the plates. There have been suggestions that some plate boundaries may bemechanically weak, especially the San Andreas fault zone, but there is no general consensus on that question yet. A fault is considered to be "weak" if its strength is smaller than about 20 MPa while a "strong" fault would have a strength in the range 50-150 MPa [*Lachenbruch and McGarr*, 1990].

The original suggestions that the San Andreas fault are probably not strong were made based on observations of heat flow and the orientation of the stress field, especially in Central California. A strong fault should give rise to a measurable heat flow anomaly over the fault zone but such a localized anomaly could not be found in heat flow measurements along the San Andreas fault [e.g., *Brune et al*., 1969; *Lachenbruch and Sass*, 1973, 1980]. In addition, it was shown more recently that the compressive stress direction lies at a high angle to the fault (65-85º) in many regions along the San Andreas fault which is inconsistent with a high-strength fault [e.g., *Mount and Suppe*, 1987; *Zoback et al*., 1987; *Lachenbruch and McGarr*, 1990].

On the other hand, there are arguments for high shear-strength of crustal materials based primarily on theoretical models for the frictional strength of fractured rock, which find laboratory-determined coefficients of friction in the range of 0.6 and 0.9 [*Byerlee*, 1978], and assume hydrostatic pore pressure. That "Byerlee's law" has been confirmed by numerous *in-situ* stress measurements in boreholes around the world. Also studies of lithospheric flexure in response to sediment, volcanic and internal loads indicate that differential stresses in much of the Earth's crust are relatively high [e.g., *McNutt*, 1980]. And finally, it has been argued that the stress indicators in Central California may not faithfully represent the direction of maximum compressive stress [*Scholz*, 2000]. He claims that the stress directions in Southern California are at a much smaller angle to the San Andreas fault (30-60º). Stress field directions in Southern California are controversial however. While *Hardebeck and Hauksson* [1999] suggested that the maximum compressive stress is about 45º in a wide zone around the fault zones, *Townend and Zoback* [2001] suggested that instead the angles cluster around 60º from the faults. The difference is apparently due to different techniques used to sample the regional seismicity [*Townend and Zoback*, 2001] when estimating the stress directions. More generally there is some concern about validity of the assumptions inherent in stress-inversion techniques such as those by *Gephardt and Forsyth* [1984] and *Michael* [1987], *viz.* the assumptions of a homogeneous stress field and of a sufficient diversity of the fault planes.

A natural way of addressing fault zone properties is to study the orientation of fault planes relative to the direction of maximum compressive stress, σ_1, since the angle between them relates to the level of shear traction acting on the fault during failure. Doing this for strike-slip events is problematic however, since the direction of σ_1 has to be estimated in the first place, and probably from the same data. On the other hand, if one of the principal stress axes is known to be vertical, the dip angle of dip-slip faults gives us that same information.

Near the surface one principal stress must indeed be vertical due to the shear-stress boundary condition at the surface [*Anderson*, 1951]. In a previous paper [*Bokelmann and Beroza*, 2000] we found that the principal strain axes as determined from focal mechanisms in Northern California are closely aligned with the vertical and the horizontal near the surface. This alignment should occur only if four conditions are met: First, the focal mechanism data set must have rather good quality, at least as good as formal errors suggest or better. Second, the stress field boundary condition must hold, making one of the three principal stress axes vertical near the surface [*Bokelmann and Beroza*, 2000]. The third condition is that failure must occur at angles of nearly 45º, and the fourth, that the faults on which failure occurs must be nearly optimally oriented with respect to the fault plane.

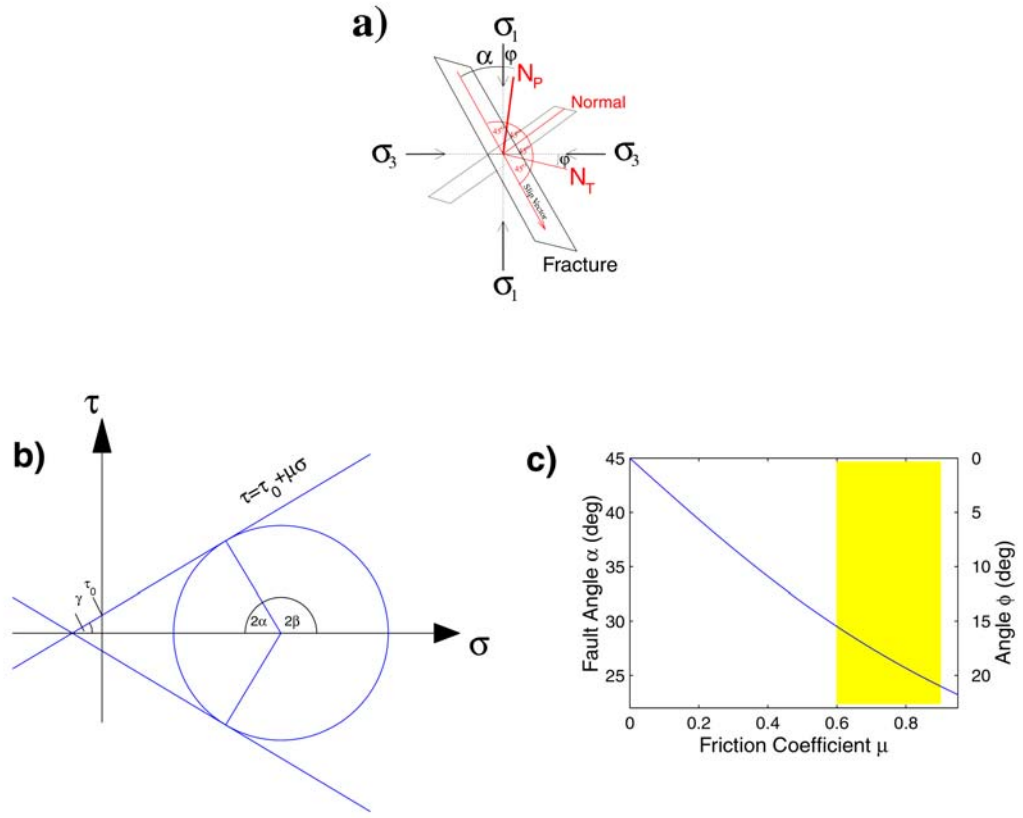

Figure 1. (a) Illustration of fracture geometry using the example of a normal fault in an Andersonian stress field σ_1 is vertical. α is the angle between the fracture and the direction of maximum compressive stress σ_1. N_P and N_T are the directions of maximum compression and maximum tension for this normal-faulting event. Both are 45º from the fracture. We analyzed measurements of $\phi = 45º - \alpha$ in this study. b) Mohr-circle for a stress state corresponding to failure on an optimally oriented set of planes. The coefficient of friction is $\mu = 0.6$ in this example. c) Dependence of the angles α and ϕ on μ. Note that α is at most 45º, which it reaches for vanishing μ. Also shown is the range of values of μ predicted from Byerlee's law (0.6-0.9).

The last two conditions are rather strong constraints on the properties of the fault zone, and we will discuss them for the near-surface region, and also what we can say about the fault properties at larger depths. We suggest that this approach gives us direct observational insight into the character of the San Andreas fault, and especially into its frictional strength. Namely, patches in the fault zone appear to be quite weak during failure, if interpreted in the context of frictional sliding.

Fracture and Friction on Faults

The general view of earthquake failure is that it is governed by friction on the fault plane. The coefficient of friction μ relates the frictional strength τ_s of the fault,

$$\tau_s = \tau_o + \mu \sigma,$$

to the (effective) normal stress σ. The angle α between σ_1 and the fault plane can take a range of values given by the part of the Mohr-circle that lies above the failure criterion. Among those angles α, α_{opt} denotes the angle of optimally oriented faults that require minimum stress difference $\sigma_1 - \sigma_3$ (diameter of circle). From the Mohr-circle in figure 1b we can infer graphically that α_{opt} is:

$$\alpha_{opt} = \pi/4 - \tfrac{1}{2} \tan^{-1}\mu$$

It is a monotonically decreasing function of μ, and is at most 45º (figure 1c). It attains that value as $\mu \rightarrow 0$.

45º is also the angle at which the *P*-axis is oriented away from the fault plane. Figure 1 shows the geometrical relationship between the fault plane, σ_1, and the *P*-axis for the example of a normal fault with σ_1 oriented vertically. Thus, for a normal faulting event the angle $\phi = 45º - \alpha = \tfrac{1}{2} \tan^{-1}\mu$ describes the deviation between the (vertical) σ_1 orientation and the *P*-axis, and we can directly infer the friction coefficient from ϕ if the faults are optimally oriented and if the principal stress axes are oriented vertically/horizontally. We will analyze measurements of ϕ below, for *P*-axes from normal faulting events, and more generally for all *P*- and *T*-axes. ϕ then takes the meaning of the angle between those axes and the vertical or horizontal orientation it would have for $\mu = 0$ (figure 2).

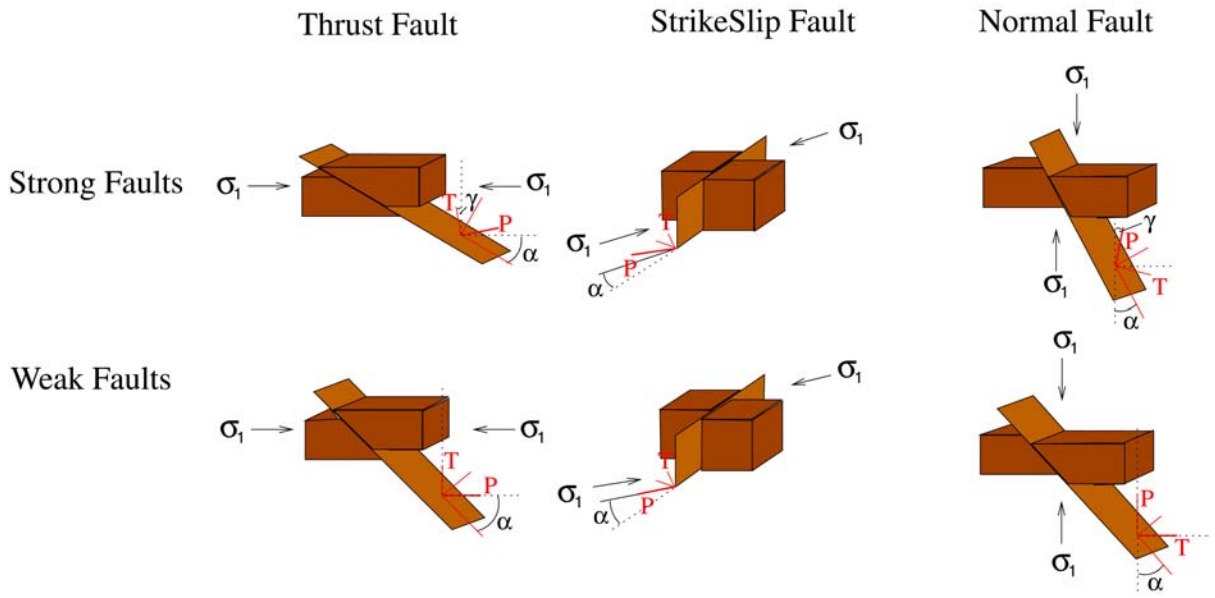

Figure 2. Optimal orientation of strong faults ($\mu \sim 0.6$) and weak faults ($\mu \sim 0$), shown separately for thrust, strike-slip, and normal faulting. Also shown are the orientations of P and T axes for the different event types. Note that these are aligned with the vertical and the horizontal in the limit of weak faults, but not for stronger faults (in the case of thrust and normal faulting).

Focal Mechanism Data

We consider seismic events between 1968 and May 1999 in northern California recorded by the Northern California Seismic Network. Out of a total of 58,884 events, we use 32,426 that are in the greater San Andreas Fault system. Within the box in Figure 3b the data sample different structural regions and several major fault zones. In this study we focus on general properties of the area within that box.

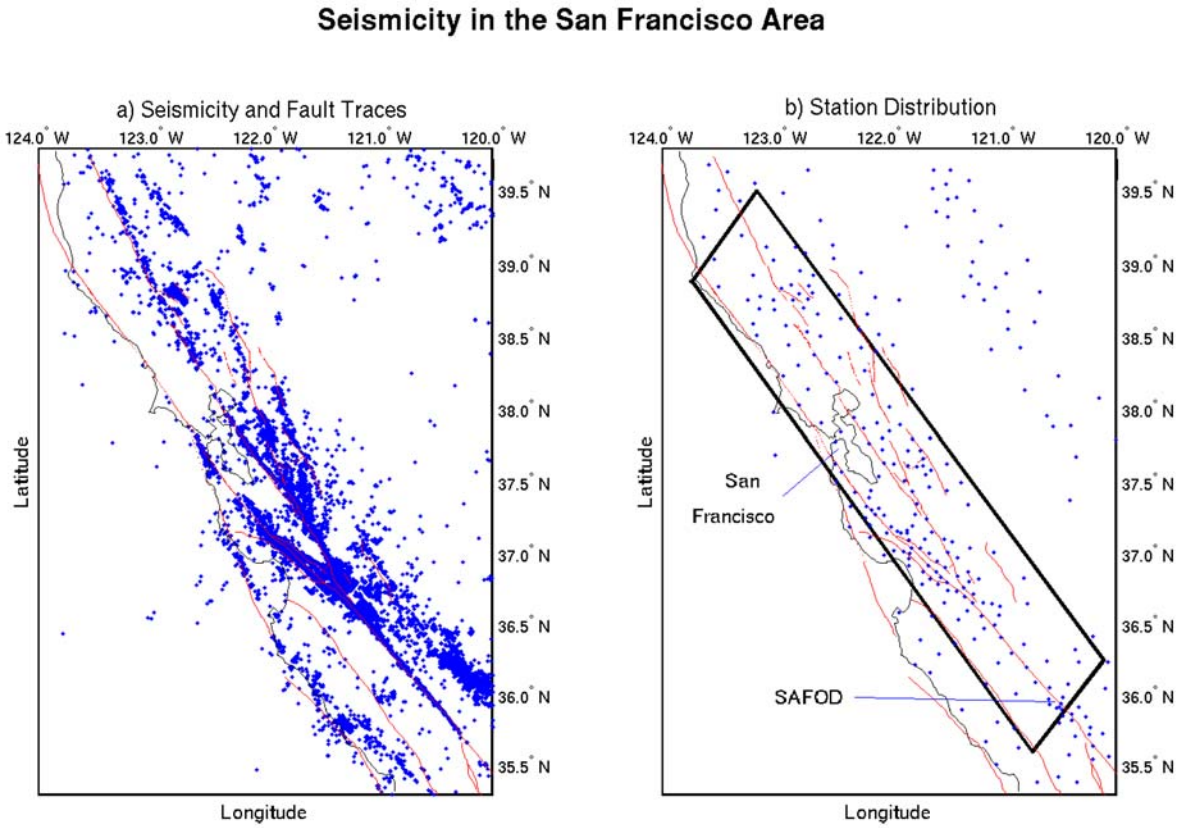

Figure 3. (a) Earthquakes and fault traces in northern California. (b) Seismic stations and fault traces. Events in this study are from the large box, which was selected based on seismic station density. SAFOD denotes the location of the proposed drilling hole into the San Andreas Fault

Focal mechanisms as well as earthquake locations were determined using a set of local velocity models to accommodate laterally varying structure [*Oppenheimer et al*, 1993]. From the subset of 32,426 events we select focal mechanisms if they satisfy a set of quality criteria that pertain primarily to formal errors of fault-plane orientation and event location,but also to the data set of first-motion observations and to parameters arising during focal mechanism inversion. These are given in *Bokelmann and Beroza* [2000], and they reduce the number of events from 32,426 to 11,326. The resulting data set is quite similar to one obtained from criteria of previous studies [*Reasenberg and Oppenheimer*, 1985; *Amelung and King*, 1997]. In the following we will consider both strike-slip and dip-slip events on or in the vicinity of the major faults, at a distance of up to 3 km from the nearest major fault. This threshold should capture most of those events, taking into account both the location uncertainty and possible dip of the fault planes.

Free Surface and the Orientation of Principal Strain Axes

We first study the orientation of the strain axes associated with the thrust faults (symbol T) and normal faults (symbol N), especially the axes of maximum shortening (subscript P) and maximum-elongation (subscript T). Figure 4 shows the inclinations of these axes. Note that for both the thrust and the normal faulting events the axes align near Earth's surface (say, the topmost two rows of panels), wherever there are data. This alignment is also very clear in the full data set [*Bokelmann and Beroza*, 2000]. Note that this alignment is not due merely to the separation in event types as thrust and normal faults, which constrain the P and T axes only weakly (to within a quadrant). At larger depth the peaks broaden substantially and the maximum of the distribution deviates from a nearly horizontal or vertical orientation in most of the panels.

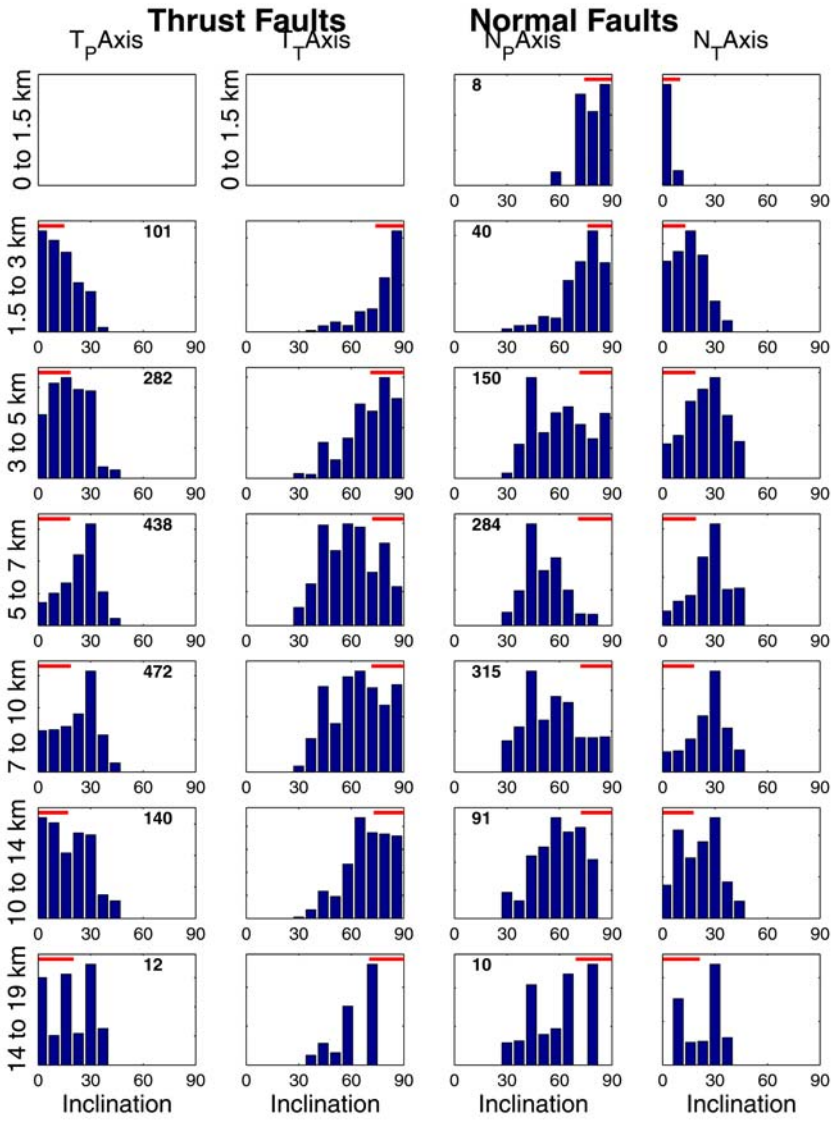

Figure 4. Orientation of principal strain axes *P* and *T* as a function of depth, for thrust-fault and normal fault quakes. For a set of depth intervals, distributions of axis inclinations $f(\phi)$ of *P* and *T* axes are shown (see text). The histograms are normalized by $\cos\phi$ to show the correct surface density on the focal sphere. Note the strong alignment near the surface with the vertical (90º) or the horizontal direction (0º). Bold numbers indicate the number of events in each depth window. Bars in each panel show the median inclination error [*Bokelmann and Beroza*, 2000]. Panels are shown only if they have at least 4 events.

The alignment near the surface can occur for a larger number of quakes only if many conditions are met, as stated in the introduction. First, the data must have rather high quality, as good as the formal errors suggest or better. Figure 4 gives the median inclination error for the respective depth interval. This error is smaller than 25° in all depth intervals, and is smallest for the panel at shallowest depth. Note that near the surface the maxima of the distributions are within that range and that the distribution width is comparable to this error, indicating that the deviation between the focal mechanisms and stress field orientation could be explained by attributing them to the measurement errors in the focal mechanisms alone.

The second condition is that one of the three principal axes must indeed be vertical. We know that this must be the case at the surface but it is unclear to what depth the free surface constrains the stress field.

The third condition is that failure in dip-slip events occurs at angles $\alpha \sim 45°$. Thus ϕ seem to be quite small.This corresponds to the case of very weak fault patches, that is, very small values of μ (figure 1c). The fourth condition is that the dip-slip patches are nearly optimally oriented. If that were not so, the α values would scatter around 45° (figure 1b).

In the following we introduce a more quantitative technique. Visual inspection of the distribution of axes orientations on the lower hemisphere, separately for each of the three event types (strike-slip, normal faulting, and thrust faulting), indicates that each is unimodal and the variation away from the maximum was about the same in every direction. This suggests an assumption that they are Fisher-distributed and that we can represent the empirical distributions in figure 4 as a marginal Fisher-distribution folded into a single quadrant (appendix A). Example distributions are shown figure 5 for a for a set of friction coefficients μ=0, μ=0.35, and μ=0.7, and a "precision parameter" κ= 100 (reciprocal variance). With increasing μ the distribution deviates more from the horizontal and vertical suggesting that we may be in principle able to determine the friction coefficient μ from the distributions of inclinations if principal stresses are vertical and horizontal for all depths. However, since the maxima of these distributions do not generally occur at 45°-½ $\tan^{-1}\mu$, we must obtain the angle ϕ that is related to the friction coefficient μ (appendix) from fitting the distributions, as well as the precision parameter κ.

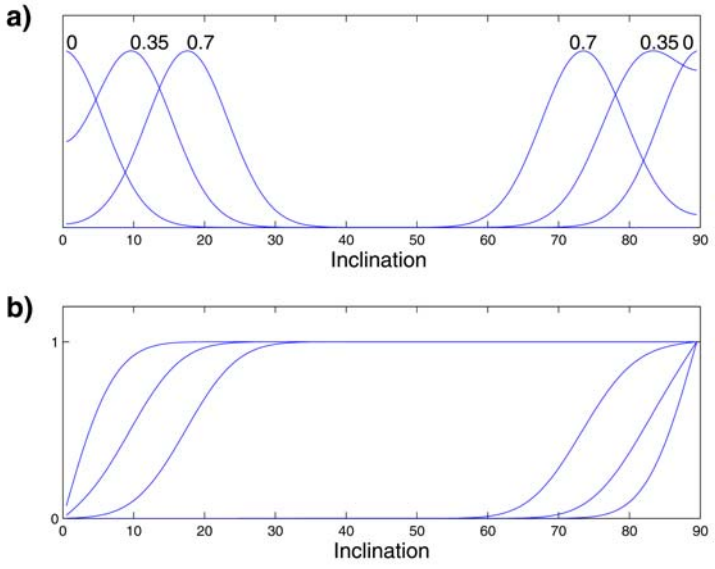

Figure 5. (a) Expected distributions of strain axes orientations shown for frictional coefficients 0, 0.35 and 0.7 and precision parameter κ = 100 (Appendix A). Each distribution is normalized by its maximum value. (b) Associated probabilities of random values to be less than θ.

Figure 5b shows cumulative probabilities associated with the distributions in figure 5a. We use these to match cumulative empirical distributions, the integrals of the histograms in figure 4. The resulting fits are shown in (figure 6).

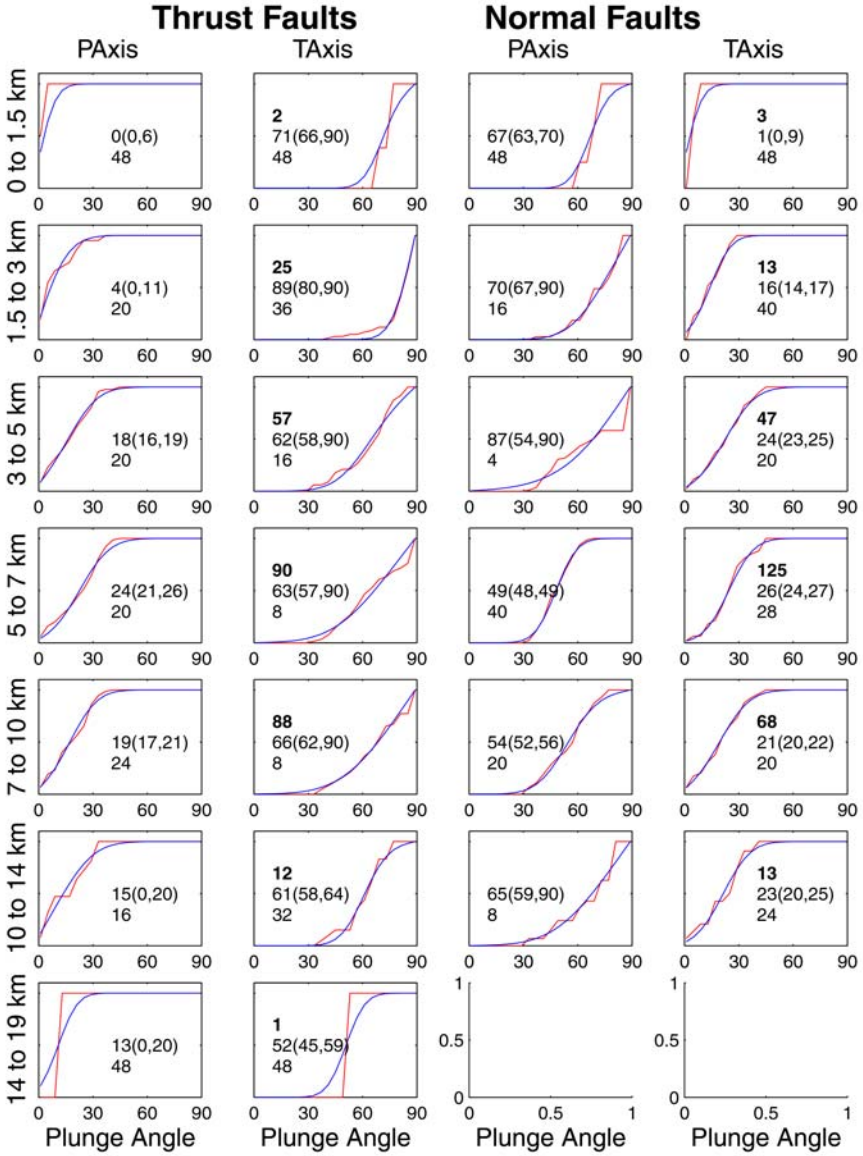

Figure 6. Fits (black) to the empirical data distributions (dotted gray) in figure 4 shown as probabilities $F(\theta)$. Numbers in the panels on the left give the resulting mode angle ϕ (and its confidence range $\phi_{\min}$ and $\phi_{\max}$) as well as the Fisher precision parameter κ (see Appendix A). N is the number of events.

The fits are generally very good except for the panels at largest depth. For each panel the resulting precision parameter κ and the optimum angle ϕ are given, the latter also with the confidence range (ϕ_{min}, ϕ_{max}). Bootstrap analysis showed that this confidence range should

correspond approximately to 1σ (Appendix A). The optimum angles ϕ are generally much better determined than the κ (figure A1), and they are shown in figure 7 as a function of depth.

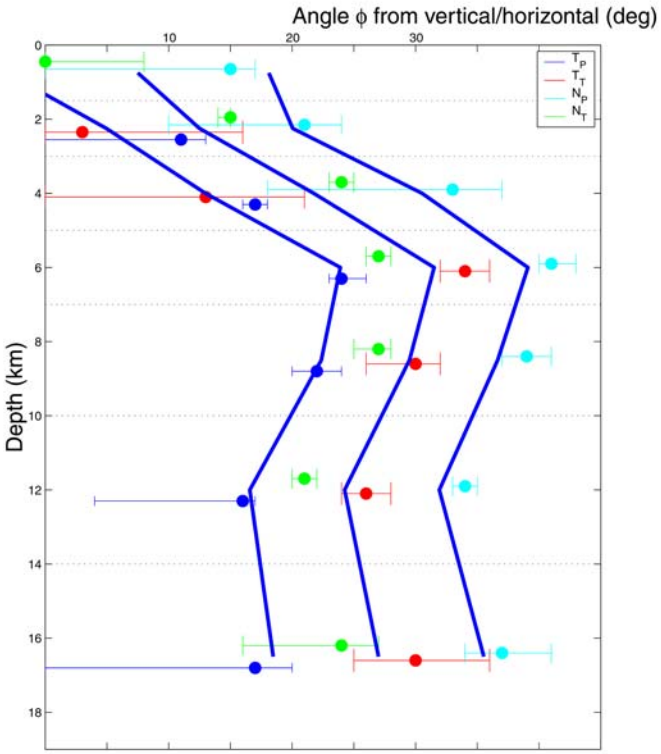

Figure 7. Range of angles ϕ consistent with the observations.

Optimum angles near the surface are in the range of 0º to 15º, and their confidence intervals range from 0º to 17º. These ϕ might be directly translated into friction coefficients, $\mu = 1/\tan(90º - 2\phi)$, if the vertical were a principal stress axis at all depths, but that only needs to hold true at the surface, while at larger depths the orientation of the nearest-vertical stress axis may differ from place to place. It is unknown to what depth the influence of the free-surface boundary condition holds, but we have constraints on the stress-field heterogeneity from the strike-slip events since their *P* and *T* axes should be nearly horizontal and unaffected by the friction coefficient (figure 2). Thus, we use the orientation of strain axes of strike-slip events to estimate to what depth the boundary condition acts, and to correct the apparent ϕ values from dip-slip events for the effect of a "non-vertical stress field". We will discuss other factors that may potentially influence the variation of ϕ later.

The *P*, *B*, and *T*-axes of the strike-slip events (S_P, S_B and S_T) were also analyzed. Their distributions show a similar behavior to the dip-slip events, with values clustering near 0º and 90º near the surface, and larger deviation at larger depths. The spread is somewhat wider than for the dip-slip events. This may be due to the uncertainties of inclinations that are larger than for the dip-slip events, which could be due to a station distribution with few or no stations above the earthquake. In such a geometry it is easier to constrain the orientation of dip-slip events than strike-slip events. The fits for the strike-slip events are at least as good as for the dip-slip events. The κ are generally smaller indicating a wider distribution of the data than for the dip-slip events. The depth distribution of angles ϕ is shown in figure 8, and is generally similar to that of

the dip-slip events with small values near the surface and largest values between 4 and 10 km. In addition, there is a decrease at the largest depth that is less apparent in the dip-slip data.

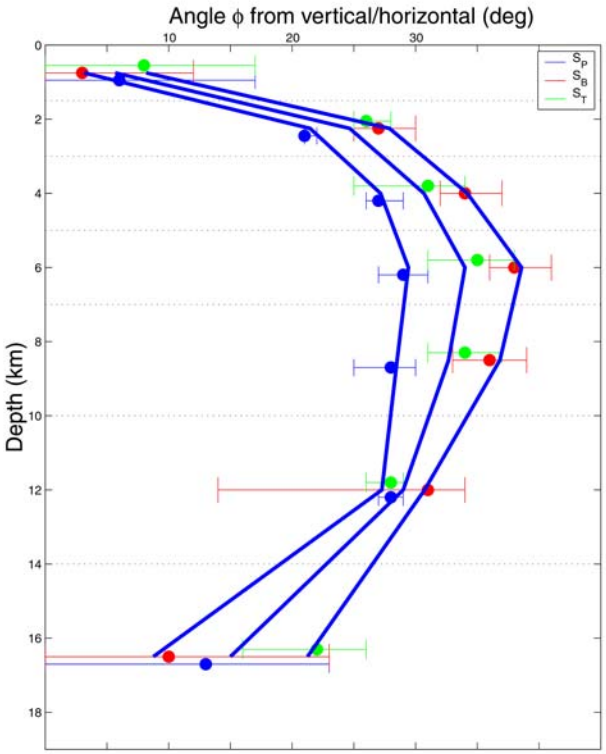

Figure 8. Ranges of angles ϕ, consistent with observations for strike-slip events.

Friction Coefficients on the San Andreas Fault

The depth-variation of $\phi_{\text{strike-slip}}$ indicates that we cannot directly interpret the corresponding $\phi_{\text{dip-slip}}$ in terms of a friction coefficient. Instead, it indicates that the vertical corresponds to a principal stress axis only down to about 3 km (and near the base of the seismogenic crust). Thus we assume that the variation of angle ϕ is due to a combination of the effects from measurement error, deviations of the stress-field from a vertical/horizontal orientation, and the friction effect that we are trying to separate. It affects only the dip-slip events strongly.

We assume that the spatial variability of the stress field with respect to the vertical orientation behaves similarly for strike-slip and dip-slip events. Figure 9 shows the allowed range of angles ϕ and associated friction coefficients that we obtain after removing the effect of "stress-field heterogeneity" from the dip-slip data (Appendix A). At depths shallower than 12 km where most of the seismicity occurs, the resulting friction coefficients are indistinguishable from zero at the 95-percent confidence level shown here. The upper bound values are near 0.3.

We can derive an upper bound for shear strength (and thus shear stress) from those values if failure is consistent with the Coulomb criterion:

$$\tau_s = \tau_o + \mu(\sigma)$$

with the measured values μ (σ) from figure 9. Figure 10 shows an upper bound of shear strength of strike-slip faults assuming that $\tau_o = 0$.

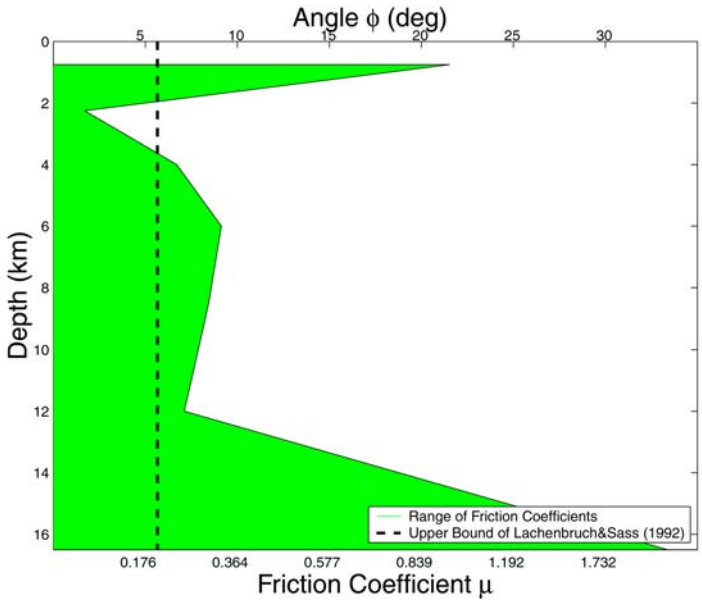

Figure 9. Allowed range of friction coefficients μ (shaded region) on the major strike-slip faults determined by correcting the axis inclinations from dip-slip events (figure 4) for the effect of "non-vertical stress-field orientation". Note the friction coefficients are probably smaller than 0.3 at depths shallower than 12 km (95 percent confidence region). This agrees roughly with the constraint of $\mu < 0.2$ (thick broken line) from *Lachenbruch and Sass* [1992].

For comparison the range of strong faults (50-150 MPa) is shown, as is the range for weak faults for $\mu < 0.2$ [*Lachenbruch and Sass*, 1992]. Note that in the depth range where most earthquakes occur (down to 12 km) the allowed range of values is nearly the same as the range for weak faults. That range was suggested by *Lachenbruch and Sass* [1992] to reconcile both the heat-flow constraint and the stress-field constraints on fault weakness. Our observation confirms that suggestion.

Discussion of Assumptions

In the above analysis we assumed that the axis inclinations are only affected by three factors, namely random errors, stress-field heterogeneity, and the friction effect. Other factors that may in principle also play a role are slip oblique to the direction of maximum resolved shear traction and non-optimally oriented fault planes.

It is generally assumed that slip is parallel to the direction of maximum resolved shear traction on the fault plane (Bott's hypothesis). This is reasonable unless there is significant mechanical anisotropy on the fault plane. Even if there were such a mechanical anisotropy this factor would be important for our study only if there were strong differences between the dip-slip and the strike-slip patches in their mechanical anisotropy, and if anything, we would expect the

perhaps better developed strike-slip patches on large-offset strike-slip faults to have less mechanical anisotropy, and consequently smaller deviations. Thus this factor does not provide a natural explanation of our observations.

We have inferred that dip-slip failure occurs on nearly optimally oriented patches near the surface. This is perhaps surprising, but if that were not the case, then we would not find such a small scatter of the principal strain axes around the vertical. This near-optimality may be explained if the material within the fault zone layer is mechanically isotropic. This is the case either if the material is intact or, more realistically, if it is pervasively fractured. We may expect faulting to occur not on a single strand but to form a complicated pattern, as has been observed for normal faulting [*Reches*, personal communication]. It is conceivable that such a developing complex fault system may be oriented optimally since there are a multitude of potential planes that the fracture may choose and it will probably choose ones that are nearly optimally oriented. We assume that the dip-slip patches are optimally oriented also at larger depth within the upper crust, or at least, that on average the dip-slip and strike-slip events show similar deviations from such an optimality, as seen in the dip angles.

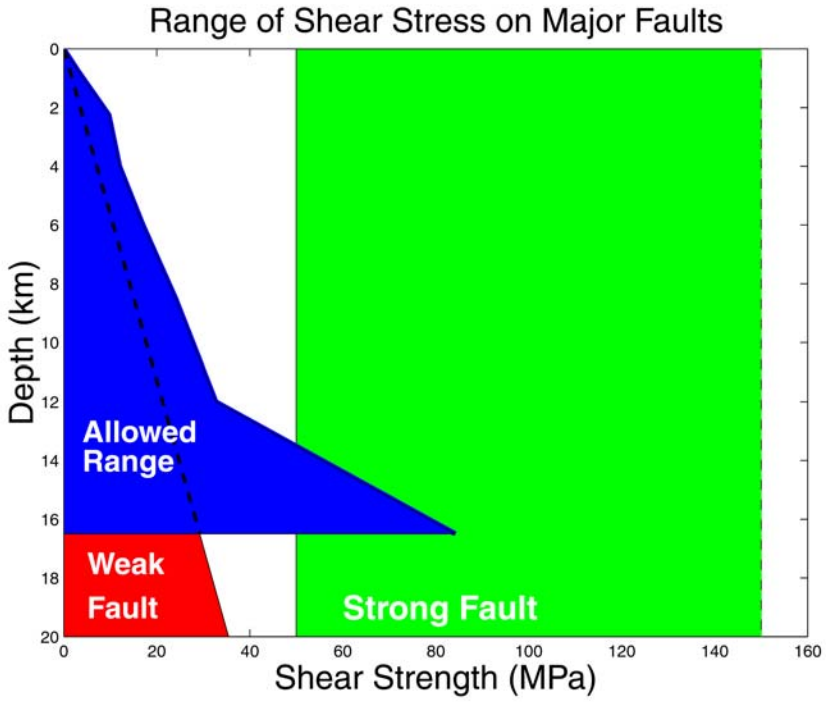

Figure 10. Range of shear stress computed from figure 9. For comparison the ranges of strong and weak faults are shown.

This seems to be in contrast with the azimuths that large faults take with respect to the stress field in the area. A number of large faults, and most prominently the San Andreas Fault, are clearly mislocated in their strike angle with respect to the stress field, which actually constitutes another argument for weakness of the fault (slip on such a misoriented fault is possible only if the fault is weak; however, we are dealing with dip angles only, and if those major strike-slip faults are vertical their dip angles are nevertheless optimally oriented. The assumption enters into our study in a weaker form, namely that strike-slip and dip-slip events may be misoriented in dip angle, but by a similar amount. If this assumption did not hold, and dip-slip events showed a misorientation in dip analogous to the misorientation in azimuth of the large strike-slip

earthquakes, then this would lead to larger apparent ϕ values for dip-slip than for strike-slip events, which we do not observe.

We also assumed that one particular property of the stress field is the same on the fault and in its vicinity where most of the dip-slip events seem to occur, that is, the mean stress field misorientation. We assumed that the effect of the free-surface boundary condition on the stress-field within the crust is expressed similarly in strike-slip and dip-slip events.

Discussion of Results

Arguments for the weakness of the major faults have been based on near-perpendicular maximum stress directions and the lack of a heat-flow anomaly. If the maximum compressive stress is nearly perpendicular to a fault that is slipping, this indicates that the faults must be weak, since the shear-stress acting on the fault must be small. This argument applies to the creeping section and to other faults that are slipping. The missing heat-flow anomaly [*Lachenbruch and Sass*, 1992] also indicated that the fault must be weak during slip, and especially for large earthquakes, because most of the dissipative heat would be generated during large events.

A few materials produce such low values of the coefficient of internal friction [*Saffer et al*., 2001] but they are thought to be unstable at higher temperature, and there are no known geologic materials that produce such low values for pressure and temperature conditions corresponding to depths of up to 12 km. Clearly, direct inspection with the San Andreas drilling at Parkfield (figure 3), and preferably deeper still, will be rather important in this context. Figure 9 predicts that the coefficient of friction on the fault (in the depth range of the borehole, down to 4 km) will be below 0.2, and the shear strength will be below 15 MPa. That coefficient of friction pertains to the scale of the seismic fracture, and it will have to be seen whether this is an intrinsic property of the material or whether perhaps scale effects [*Hoek and Brown*, 1980; *Pinto da Cunha*, 1990] are important to explain the weakness.

Small values of μ have also been found by *Iio* [1997] by studying focal mechanisms in Japan, and normal faulting events also seems to often have angles of about 45º with the vertical [*Colletini and Sibson*, 2001], which may also suggest low coefficients of friction. This is consistent with laboratory data for higher confining pressures where the ductile deformation becomes independent of normal stres. For typical lab materials such small values of μ are found, although at somewhat larger confining pressures [e.g., *Shimamoto*, 1986]. Our data suggest that such low values can occur at lower stress within fault zones.

Another way of explaining the main observation of this paper, that faulting seems to occur mostly in the direction of τ_{max} is by invoking plastic flow. Following *Saint-Venant* [1870] one can show that deformation associated with plastic flow is parallel to τ_{max}. This raises the question of whether plastic flow could play an important role in faulting in upper-crustal fault zones. A number of authors have argued that this is the case [e.g., *Byerlee and Savage*, 1992; *Roberts and Turcotte*, 2000]. In fact, we observe plastic deformation directly as fault creep, e.g., in the Creeping Section. It has also been shown that plastic instability can lead to earthquakes [*Hobbs et al*., 1986], and this is may help to explain the occurrence of earthquakes in the lower crust.

Conclusions

This study attempts to shed some light on the strength or weakness of the San Andreas fault and its possible cause. Our approach is to study the depth-dependent orientation of fault planes as determined by seismological data, and to infer the coefficient of friction.

We find small values of the friction coefficient at essentially all depths in the upper crust where seismicity occurs. The data suggest that the major faults in Northern California are weak,

as was suggested previously based on the missing heat-flow anomaly and nearly fault-normal direction of the maximum compressive stress.

In fact, the range of friction coefficients we obtain in this study is quite similar to the range of values that was claimed by *Lachenbruch and Sass* [1992] in order to reconcile both heat-flow data and stress constraints $\mu < 0.2$. Such values are obtained for fault zone materials in laboratory experiment at low pressure and temperature, but it is less clear how to explain these values for higher temperatures, since most intrinsically weak materials are unstable at the temperatures acting at depths larger than a few km. The San Andreas Fault Observatory at Depth experiment may help to resolve these issues. Our prediction is that intrinsic friction in the depth range of the borehole (up to 4 km depth) will be smaller than 0.2.

Appendix: Marginal Fisher Distribution

The basic model for a unimodal distribution of directional data in 3D is the Fisher density distribution in the general form

$$h(\theta,\phi)dS = \kappa e^{\kappa(\sin\theta\sin\phi\cos(\eta-\beta)+\cos\theta\cos\phi)} / (4\pi\sinh\kappa)\ dS$$

[*Fisher*, 1953; *Fisher et al*., 1987] for azimuth η and inclination θ ($0 < \theta \leq \pi$; $0 \leq \eta < 2\pi$). The Fisher-distribution has 3 parameters (ϕ,β,κ). $\theta = \phi$ and $\eta = \beta$ give the location of the mode (maximum) and κ is the "precision parameter" that describes the degree of concentration around the mode. A uniform distribution on the sphere corresponds to a value of $\kappa = 0$.

Since we are studying distributions of inclinations only (not azimuths) we are interested in the marginal distribution

$$g(\theta) = \int h(\theta,\eta)d\eta$$

Where the limits of integration run from 0 to 2π. We can give this for the standardized form, that is for $\phi = 0$:

$$g(\theta) = \kappa e^{\kappa\cos\theta} / 2\sinh\kappa$$

In our case ϕ will not usually be zero, and we need to solve the integral. The equation immediately above gives the surface density on the sphere, taking into account the inclination-dependent size of the surface-element: $dS = d\theta\, d\phi \sin\theta$.

Based on the marginal Fisher distribution $g(\theta)$ figure 6 shows a set of functions:

$$f(\theta) = g(\theta) + g(\pi-\theta),\ 0 < \theta < \pi/2,$$

that simulate the deviation of stress-axes from a normal and vertical orientation for a set of Fisher-distributed stress axes. The parameters in this example are $\kappa = 100$ and with $\phi = 0°$ ($\mu = 0$), $\phi = 9.65°$ ($\mu = 0.35$), $\phi = 17.45°$ ($\mu = 0.7$). If $\phi = 0°$ (90°), then the maximum is at ϕ. For

other ϕ the maximum deviates slightly from ϕ but the deviation is small unless κ is very small. Figure 6 also shows the associated probability distribution for a random value $x < \theta$ to occur.

For a given data distribution we obtain the two parameters ϕ, and κ by fitting predicted cumulative probability distributions $F(\theta)$ to the empirical ones, and by minimizing the quadratic misfit. The uncertainty of the mode may be obtained by projecting the confidence region at the chosen significance level (figure A1), here 4σ, and by scaling the confidence level using a bootstrap technique.

Another property of the distribution $f(\theta)$ that we will make use of is that the sum c=a+b of two f-distributed random variables which have parameters (ϕ_a, κ_a) and (ϕ_b, κ_b) has parameters (ϕ_c, κ_c) and $\phi_c \approx \phi_a + \phi_b$. We confirmed numerically that this holds to within a few degrees in the parameter ranges of interest for this study.

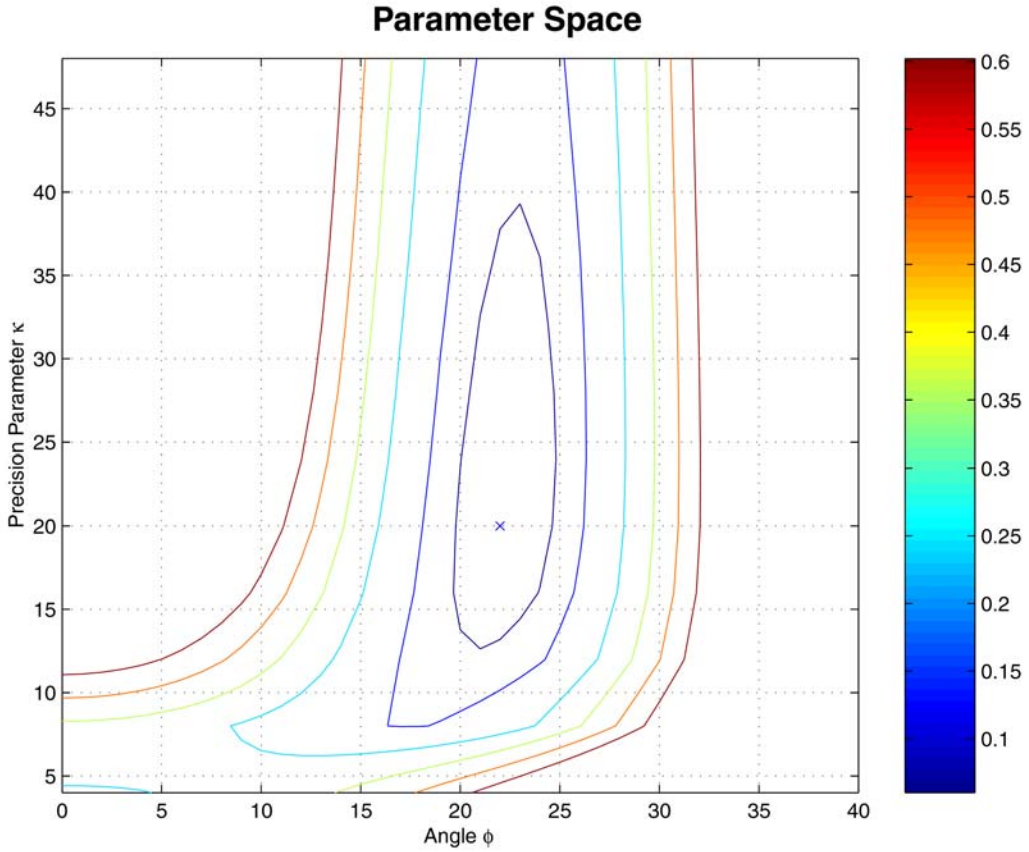

Figure A1. Parameter space of mode angle ϕ and precision parameter κ, for T_P (7-10 km). Contours are shown for S_{crit} corresponding to 4σ (unscaled, see Appendix), and 2, 3, 4, 5, and 6 times S_{crit}. The best-fitting model is shown by an "x".

References

Amelung, F., and G. King, Large-scale tectonic deformation inferred from small earthquakes, *Nature*, 386, 702-705, 1997.

Anderson, E.M., *The Dynamics of Faulting*, Oliver and Boyd, White Plains, N.Y., 1951.

Bokelmann, G.H.R., Beroza, G.C., Depth-dependent earthquake focal mechanism orientation: Evidence for a weak zone in the lower crust, *J. Geophys. Res*, 105, 21683-21696, 2000.

Brune, J.N., T.L. Henyey and R.F. Roy, 1969, Heat flow, stress, and rate of slip along the San Andreas fault, California*, J. Geophys. Res*., 74, 3821-3827.

Byerlee, J.D., Friction of rocks, *PAGEOPH*, 116, 615-629, 1978.

Fisher, R. A. 1953. Dispersion on a sphere, *Proceedings of the Royal Society of London Series A,* 217, 295-305, 1953.

Fisher, N.I., Lewis, T., Embleton, N.J.J., 1987, Statistical analysis of spherical data, Cambridge University Press, 1987.

Gephart, J.W., and D.W. Forsyth, An improved method for determining the regional stress tensor using earthquake focal mechanism data: Application to the San Fernando earthquake sequence, *J. Geophys. Res.,* 89, 9305-9320, 1984.

Hardebeck, J.L., Hauksson, E., Role of fluids inferred from stress field signatures,

Science 285, 236-239., 1999.

Hoek, E., Brown, E.T., Underground excavations in rock, Inst. Mining and Metallurgy, London. Inst. Mining and Metallurgy, London., 1980.

Jaeger, J.C., Cook, N.G., *Fundamentals of Rock Mechanics*, Chapman and Hall, London, 1969.

Lachenbruch, A.H., A. McGarr, Stress and heat flow, in: The San Andreas Fault System,

ed. by R. Wallace, *USGS Professional Paper 1515*, 1990.

Lachenbruch, A.H., and J.H. Sass, Thermo-mechanical aspects of the San Andreas Fault system, in *Proceedings of the Conference on Tectonic Problems of the San Andreas Fault System*, pp. 192-205, Stanford Univ. Press, Stanford, Calif., 1973.

Lachenbruch, A.H. J.H. Sass, Heat flow and energetics of the San Andreas fault zone, *J. Geophys. Res.*, 85, 6185-6223, 1980.

Lachenbruch, A.H., J.H. Sass, Heat flow from Cajon Pass, fault strength, and tectonic implications, *J. Geophys. Res.,* 97, B4, 4995-5015, 1992.

McGarr, A., and N.C. Gay, State of stress in the Earth's crust, *Ann. Rev. Earth Planet. Sci., 6,* , 405-436, 1978.

McKenzie, D.P., The relation between fault plane solutions for earthquakes and the directions of the principal stresses, *Bull. Seismol. Soc. Am.,* 59, 591-601, 1969.

McNally, K.C., and T.V. McEvilly, Velocity contrast across the San Andreas Fault in central California: Small-scale variations from *P*-wave nodal plane distortion, *Bull. Saeismol. Soc. Am.,* 67, 1565-1576, 1977.

McNutt, M., Implications of regional gravity for state of stress in the Earth's crust and upper mantle, *J. Geophys. Res*., 85, 6377-6396, 1980.

Michael, A.J., Use of focal mechanisms to determine stress: a control study, *J. Geophys. Res.,* 92, 357-368, 1987.

Mount, V.S. and J. Suppe, State of stress near the San Andreas fault: Implications for wrench tectonics, *Geology*, 15, 1143-1146, 1987.

Oppenheimer, D., F. Klein, J. Eaton, and F. Lester, The northern Californian seismic network bulletin, January-December 1992, *U.S.Geol. Surv. Open File Rep., 93-578*, 1993.

Pinto da Cunha, A. (ed.),Scale Effects in Rock Masses, Proc. 1st ISRM Int. Workshop, Scale Effects in Rock Masses, Proc. 1st ISRM Int. Workshop, Loen, Norway, 352 p. AA Balkema, Rotterdam, 1990.

Reasenberg, P.A., D.H. Oppenheimer, FPFIT, FPPLOT and FPPAGE; Fortran computer programs for calculating and displaying earthquake fault-plane solutions, *U.S. Geol. Surv. Open File Rep., 85-739*, 1985.

Saffer, D.M., Frye, K.M., Marone, C., Mair, K., Laboratory results indicating complex and potentially unstable frictional behavior of smectite clay, *Geophys. Res. Lett.*, 28, 12, 2297-2300, 2001.

Schaff, D. P., G. H. R. Bokelmann, G. C. Beroza, F. Waldhauser, and W. L. Ellsworth, High resolution image of Calaveras Fault seismicity, *J. Geophys. Res*., **107** (B9), 2186, doi:10.1029/2001JB000633, 2002.

Scholz, CH, Evidence for a strong San Andreas fault, *Geology*, 28, 163-166, 2000.

Shimamoto, T., 1986, A transition between frictional slip and ductile flow undergoing large shearing deformation at room temperature, *Science*, 231, 711-714, 1986.

Townend, J., and Zoback, M. D., Implications of earthquake focal mechanisms for the frictional strength of the San Andreas fault system. In R.E. Holdsworth, R. A. Strachan, J. Macloughlin, and R. J. Knipe (eds.), The Nature and Tectonic Significance of Fault Zone Weakening. *Special Publication of the Geological Society of London*, 186 , 13-21, 2001. .

Zoback, M.D., et al., New evidence on the state of stress of the San Andreas fault system,*Science*, 238, 1105-1111, 1987.